metals

MDPI

Article

The Cyclic Stability of Superelasticity in Aged $Ti_{49.3}Ni_{50.7}$ Single Crystals with Oxide Surface

Anna S. Eftifeeva [1,*], Elena Y. Panchenko [1], Ilya D. Fatkullin [1], Mikhail N. Volochaev [2], Anton I. Tagiltsev [1] and Yuriy I. Chumlyakov [1]

[1] Laboratory for Physics of High-Strength Crystals, Siberian Physical-Technical Institute, Tomsk State University, Lenina Str. 36, 634050 Tomsk, Russia
[2] Kirensky Institute of Physics, Siberian Branch, Russian Academy of Sciences, Akademgorodok 50/38, 660036 Krasnoyarsk, Russia
* Correspondence: a.s.eftifeeva@mail.tsu.ru

Abstract: The cyclic stability of superelasticity in compression in $[001]_{B2}$-oriented $Ti_{49.3}Ni_{50.7}$ single crystals is considered in this paper. The crystals were aged at 823 K for 1.0 h in air and helium. It has been experimentally shown that a two-layered surface thin film, consisting of a Ni-free oxide layer and a Ni-rich sublayer, appears after the oxidation at 823 K in air. The surface layers have a weak effect on the forward B2-R-B19′ martensitic transformation temperatures: T_R temperature increases by 4 K; M_s and M_f temperatures decrease by 6 K. The oxide layer does not affect either the superelasticity response during fatigue tests or the temperatures of reverse B19′-B2 martensitic transformation. The cracking of the surface oxide layer during fatigue tests was not found in $[001]_{B2}$-oriented single crystals aged in air. This is contributed by the relaxation of internal stresses. Such internal stresses are caused by both the formation of an oxide layer during aging and the matrix deformation at the stress-induced martensitic transformation. The main relaxation mechanisms of the internal stresses are the oriented growth of Ti_3Ni_4 precipitation near a thin surface film at aging in air, the formation of dislocations near the precipitation-matrix interface and a fine twinned B19′-martensite at fatigue tests.

Keywords: martensitic transformation; single crystals; aging; precipitation; oxide layer; functional properties

Citation: Eftifeeva, A.S.; Panchenko, E.Y.; Fatkullin, I.D.; Volochaev, M.N.; Tagiltsev, A.I.; Chumlyakov, Y.I. The Cyclic Stability of Superelasticity in Aged $Ti_{49.3}Ni_{50.7}$ Single Crystals with Oxide Surface. *Metals* **2022**, *12*, 2113. https://doi.org/10.3390/met12122113

Academic Editor: Chonghe Li

Received: 31 October 2022
Accepted: 6 December 2022
Published: 8 December 2022

1. Introduction

TiNi-based shape memory alloys (SMAs) are widely used in engineering and medicine as functional materials of a new generation owing to the combination of the shape memory effect (SME), superelasticity (SE), high plasticity, biocompatibility and corrosion resistance [1–3]. The SME and SE are effectuated by reversible B2-R-B19′ martensitic transformations (MTs) in these alloys.

The SME and SE of NiTi binary alloys are sensitive to thermomechanical treatments, which are used as a means of controlling the properties of these alloys due to the microstructure change (particles precipitation) [4–7]. Also, TiNi alloys have been known to react vigorously with oxygen at elevated temperatures to form titanium oxide TiO_2 (rutile). The formation of titanium oxide on the surface of biomedical TiNi implants improves their corrosion resistance as well as biocompatibility by eliminating nickel from the surface, which is known to be toxic and allergenic in Ni-sensitive patients [8–17]. Thus, the achievement of optimal SME and SE due to the particles precipitation together with the modification of the NiTi alloys surface with a protective oxide layer is topical to working out the medical TiNi-based materials.

Most of the previous studies of the TiNi alloy with an oxide layer have concerned medical applications and focused on the identification of oxidation products, oxidation kinetics and corrosion resistance [9–14,18]. References [10,12–14,17] show that the oxidation temperature above 873 K is not effective. In this case, the thick oxide layer (more than

100 μm), which consists of a porous phase with a rough aspect, is formed. It cracks off the sample surface exposing an underneath Ni-rich layer, dangerous for Ni-sensitive patients. At the same time, a smooth protective oxide layer is formed upon oxidation at temperatures of 673–873 K. Only several studies of MT temperatures and internal stress fields in oxidized TiNi alloys are known [13,14]. To the best of our knowledge, the influence of the thin oxide layer on the SME, SE and their cyclic stability in bulk samples of TiNi alloy has not been thoroughly studied. Nevertheless, it is impossible to use the material in biomedicine without elucidating the effect of the surface layer on the operational properties. So, the purpose of this work is to find out the influence of the oxide layer on the cyclic stability of SE in compression in aged $Ti_{49.3}Ni_{50.7}$ single crystals oriented along the $[001]_{B2}$-direction.

2. Materials and Methods

The $Ti_{49.3}Ni_{50.7}$ single crystals were produced by the Bridgman technique. The samples were cut from single-crystals on an electrospark machine (wire-cutting machine) Arta 153 (OOO NPK Delta-Test, Fryazino, Russia). The dimensions of the samples for compressive tests were $3 \times 3 \times 6$ mm^3. The hardened surface after the samples' cutting was removed by chemical etching. Then the samples' surface was mechanically ground and electrolytically polished. The samples were annealed at 1253 K for 1.0 h followed by water quenching. Next, they were aged at 823 K for 1.0 h in helium (marked as without oxide layer) and in air (marked as with oxide layer). Such heat treatment was chosen based on our previous studies and those of other scientific groups [10,12–14,17,19,20]. The samples' surface after aging in helium was mechanically ground and electrolytically polished again to precisely prevent the formation of an oxide film on the surface.

The samples had orientations of compressive axes near the $[001]_{B2}$ with a deviation from the pole of 10°. The long side of the sample coincides with the compressive axis. The normals to the side surface of the sample were $[110]_{B2}$ and $[\bar{1}10]_{B2}$. Such compression axis was chosen due to the fact that the $[001]_{B2}$-oriented crystals should possess high-strength properties of the B2-phase and perfect SE response in compression since the Schmid factor for the <001> {110} slip system of B2 phase is zero [4,19,21]. The contribution of martensite detwinning to the transformation strain in compression is minimal, and the theoretical B2-R-B19′ transformation strain for studied orientations is $\varepsilon_0 \approx 5.0\%$ [19].

The SE parameters of critical stresses for the stress-induced martensite formation σ_{cr}, stress hysteresis $\Delta\sigma$ and reversible strain ε_{rev} were determined from the $\sigma(\varepsilon)$ curves. The value of critical stresses σ_{cr} was determined as a yield strength $\sigma_{0.1}$, (by analogy with plastic deformation by slipping or twinning) taken at 0.1 % of plastic strain. The stress hysteresis $\Delta\sigma$ was determined in the middle of the SE loop as the stress difference between the forward and the reverse stress-induced MT. The SE value ε_{rev} was defined based on the elastic moduli of the forward and reverse MT at the stress level σ_{cr}.

The microstructure of single crystals and the chemical composition of the oxide layer were studied on a transmission electron microscope (TEM) HT-7700 (Hitachi, Tokyo, Japan). Oxidized surface and nearby microstructure were studied in the cross-sectional foil (perpendicular to the $[001]_{B2}$ compression axis) prepared by focused ion beam (FIB). Structure degradation mechanisms were studied on disks with a diameter of 3 mm and a thickness of 100 μm that were finally prepared using double-jet electrochemical polishing by a Tenupol-5 (Struers, Ballerup, Denmark). The chemical composition was determined by energy dispersive X-ray spectroscopy (EDS) XFlash 6T/60 (Bruker, Berlin, Germany). The MT temperatures were determined by differential scanning calorimetry (DSC) using a DSC 404F1 Pegasus (NETZSCH, Bayern, Germany). The loading/unloading cycles were performed using a VHS 5969 universal testing machine (Instron, High Wycombe, UK). Errors in strain and stress measurements during mechanical tests were 0.2 % and 2 MPa, respectively. The strain rate during the study of SE response was $2.0 \cdot 10^{-3}$ s^{-1}.

3. Results

A scanning transmission electron microscope (STEM) image and a distribution of chemical elements in the cross section of oxidized samples are shown in Figure 1. The samples were aged at 823 K for 1.0 h in air.

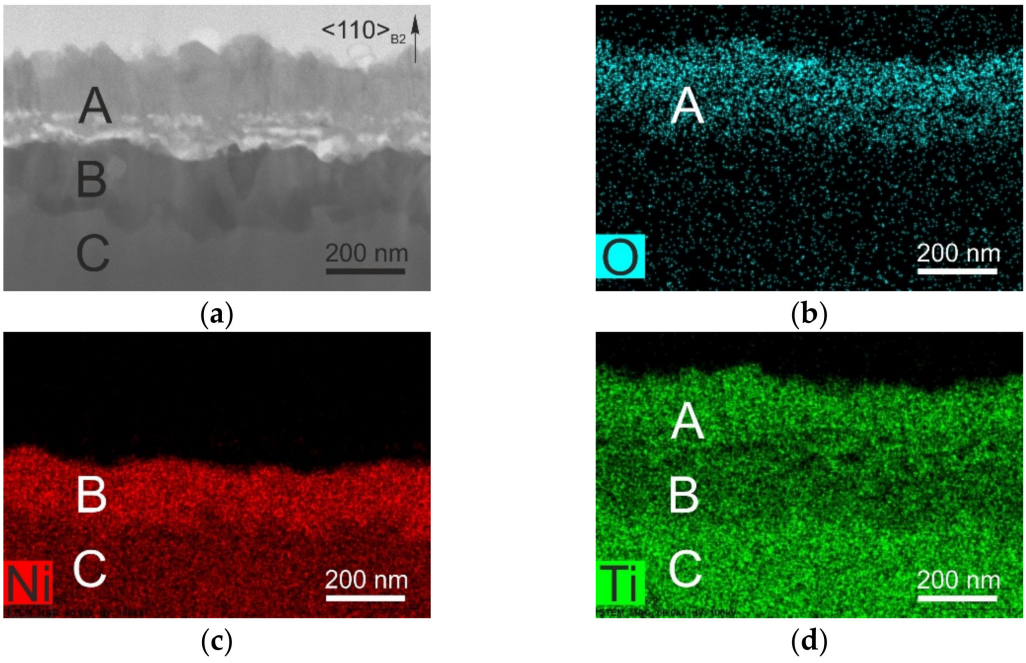

Figure 1. (**a**) STEM image and (**b**–**d**) chemical mapping of the cross sections of $Ti_{49.3}Ni_{50.7}$ single crystals aged at 823 K for 1.0 h in air.

The surface film formed due to aging in air is characterized by a gradient change in the elemental composition with depth, which indicates the formation of a diffusion transition between the oxide layer region and the B2-matrix (Figure 1a). The surface film with thickness up to 420 nm is a multilayer system. The outer A layer with a thickness of 250 nm is Ni-free (the Ni content does not exceed 0.3(±0.1) at. %) with amorphocrystaline structure. The A layer is enriched with O (78.0(±1.9) at. %) and contains Ti (21.8(±0.6) at. %) (Figure 1b–d). It is known that the Ni-free layer is identified as titanium oxide TiO_2 (rutile) [9–14,18]. The formation of pores is possible at the bottom of the oxide layer A (bright areas in Figure 1a).

Between the surface oxide A layer and the matrix of $Ti_{49.3}Ni_{50.7}$ alloy (marked as C), the B sublayer is located (Figure 1a). In the B sublayer, the predominant element is Ni so that the Ti/Ni ratio is 1:3 (75.5 at. % Ni, 24.5 at. % Ti) (Figure 1b–d). The Ni-rich B sublayer is thinner than an oxide A layer by 1.5 times, and the thickness of the B sublayer is up to 170 nm. The Ni-rich layer is identified as the $TiNi_3$ phase [9–14,18]. The intensity curve of oxygen is low compared to the predominant Ti and Ni elements in layer B, so the EDS method cannot determine the quantitative value of oxygen properly.

The DSC analysis showed that aged $Ti_{49.3}Ni_{50.7}$ single crystals undergo a two-stage B2-R-B19′ MT both without and with an oxide layer (Figure 2, Table 1). The existence of the R-phase is characteristic of aged TiNi alloys containing dispersed Ti_3Ni_4 particles [21].

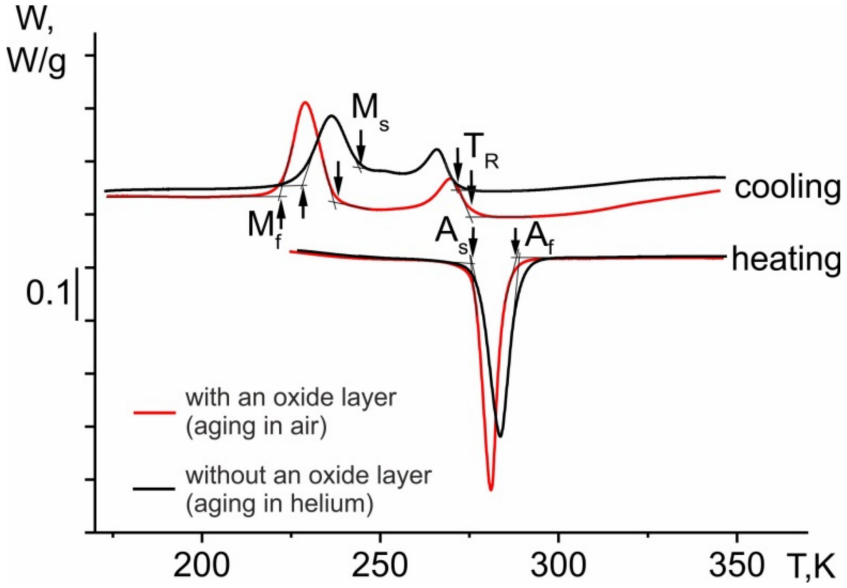

Figure 2. DSC curves during cooling/heating for $Ti_{49.3}Ni_{50.7}$ single crystals aged at 823 K for 1.0 h in air and helium.

Table 1. The B2-R-B19′ MT temperatures in $Ti_{49.3}Ni_{50.7}$ single crystals aged at 823 K for 1.0 h in air and helium.

Single Crystals	M_s (±2), K	M_f (±2), K	A_s (±2), K	A_f (±2), K	T_R (±2), K	ΔT (±2), K
with an oxide layer (aging in air)	238	221	276	288	275	50
without an oxide layer (aging in helium)	244	227	277	289	271	45

It can be seen that an oxide layer reduces the temperatures of the forward R-B19′ MT M_s and M_f by 6 K, increases the temperature T_R by 4 K and thermal hysteresis ΔT by 5 K compared to the crystals without the layer. The surface oxide layer does not affect the temperatures of the reverse B19′-B2 MT A_s and A_f (Figure 2, Table 1).

The results of cyclic testing of aged $Ti_{49.3}Ni_{50.7}$ single crystals with and without an oxide layer are shown in Figure 3. Compressive fatigue testing has been received in the conditions of the complete reversible stress-induced MT: stress level under loading of 550 MPa, test temperature of T = 295 K > A_f.

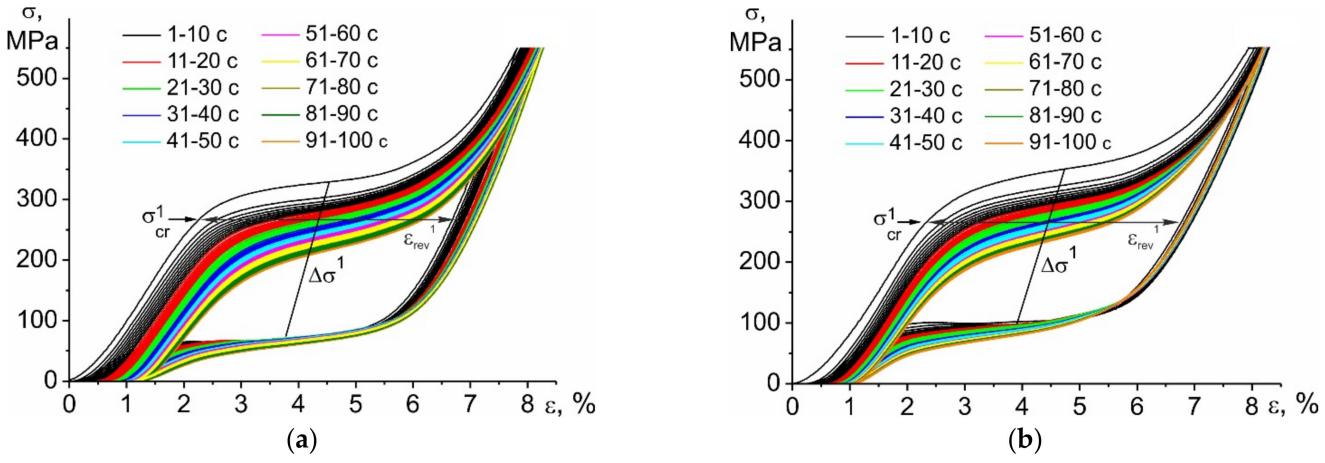

Figure 3. Cyclic stress-strain responses at T = 295 K for $Ti_{49.3}Ni_{50.7}$ single crystals aged at 823 K for 1.0 h (**a**) in air and (**b**) in helium.

The analysis of the presented data shows that [001]B2-crystals with and without an oxide layer are characterized by the same compressive functional fatigue responses during the loading/unloading cycles from 1 to 100. The complete stress-induced MT in the 1st cycle (n = 1) occurs at critical stress of martensite formation σ_{cr} = 265–267 MPa with the stress hysteresis $\Delta\sigma$ = 252–262 MPa and reversible strain ε_{rev} = 4.6–4.8 % (Figure 3).

It can be seen from Figures 3 and 4 that with an increase in the number of cycles the evolution of SE curve is observed. The degradation of SE parameters (critical stress martensite formation σ_{cr}, stress hysteresis $\Delta\sigma$, reversible strain ε_{rev}) takes place, and the irreversible strain accumulates. In $[001]_{B2}$-single crystals aged both in air and helium, the significant changes of SE parameters occur in the first 30 cycles. The critical stresses σ_{cr}, stress hysteresis $\Delta\sigma$ and reversible strain are reduced, respectively, by 73–77 MPa, by 65–72 MPa and by 0.5 % in 30th cycle compared with the 1st cycle for $[001]_{B2}$-crystals with and without an oxide layer (Figure 4). Thus, with an increase in the number of cycles from n = 1 to n = 30, the SE parameters (σ_{cr} and $\Delta\sigma$) decrease by 30%, and the irreversible strain accumulates together with reducing the reversible strain (Figures 3 and 4). Significant SE degradation in the first loading/unloading cycles is typical for TiNi polycrystals and single crystals [5,22–24].

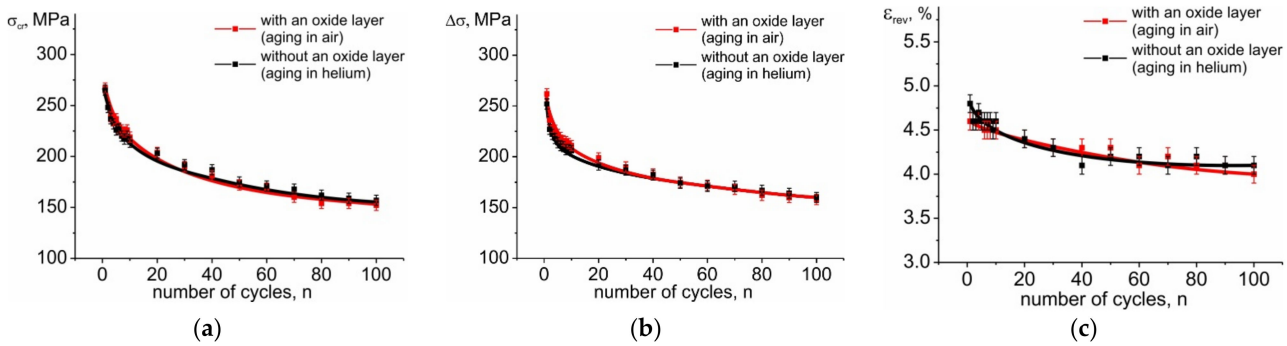

Figure 4. Dependence of SE parameters ((**a**) critical stress of martensite formation σ_{cr}, (**b**) stress hysteresis $\Delta\sigma$, (**c**) reversible strain ε_{rev}) on the number of cycles n for $Ti_{49.3}Ni_{50.7}$ single crystals aged at 823 K for 1.0 h in air and in helium.

Further, the SE curves gradually change from 30 to 100 cycles. The critical stress is σ_{cr} = 152–157 MPa, and the stress hysteresis is $\Delta\sigma$ = 158–160 MPa in 100th cycle for $[001]_{B2}$-crystals with and without an oxide layer (Figure 4). The SE parameters (σ_{cr} and $\Delta\sigma$) decrease by 15–20%, with increasing in the number of cycles from n = 30 to n = 100. The irreversible strain does not increase, and the reversible strain changes slightly at n = 30–100 (Figures 3 and 4).

4. Discussion

Nam and colleagues [14] found that the temperatures of the B2-B19′ (R-B19′) MT increase with the growth of oxide layer in TiNi-based alloys. They suggested that the increase of the transformation temperatures is attributed to a compressive stress induced by this oxide layer. Indeed, it is known that both the external applied stresses and the internal stresses (for example, arising one from the oriented growth of dispersed Ti_3Ni_4 particles) lead to the increase in the temperatures of forward and reverse MT as described by the Clausius–Clapeyron relationship [25–27]. In this study, it was found that the temperatures of forward MT decrease by 6 K (which is close to the measurement error of ±2 K), and the temperatures of reverse MT do not change in single crystals with an oxide layer compared to the crystals without such layer (Figure 2, Table 1). It is assumed that the formation of an oxide layer together with Ti_3Ni_4 particles during aging in studied $Ti_{49.3}Ni_{50.7}$ single crystals is the possible reason of a weak effect of the oxide layer on the MT temperatures (Figure 2, Table 1).

It is known [4,19,21] that four variants of Ti_3Ni_4 particles with a $\{111\}_{B2}$ habit plane are precipitated in the TiNi alloy after aging without applied stress, which is observed in the studied single crystals aged in air away from the surface and in helium (Figure 5). The $<111>_{B2}$-directions are located symmetrically relative to the $[001]_{B2}$-direction. The angle between directions of the $[001]_{B2}$ compression axis and the normal to the habit plane of particles $<111>_{B2}$ is 54.7° for all crystallographic variants of Ti_3Ni_4 particles. The lens-shaped Ti_3Ni_4 particles with a length of 300–400 nm occupy 12–13% of the volume fraction of the B2-matrix of investigated crystals aged in air and in helium (Figure 5). These precipitates do not undergo B2-R-B19′ MT and are deformed only elastically.

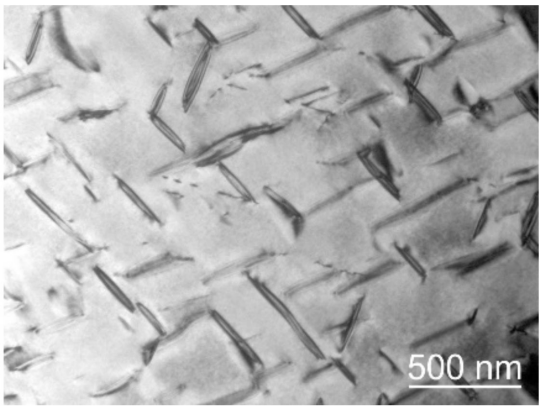

Figure 5. TEM study of $Ti_{49.3}Ni_{50.7}$ single crystals aged at 823 K for 1.0 h in helium before fatigue tests.

A detailed TEM study of single crystals aged in air (with an oxide layer) showed that the oriented growth of Ti_3Ni_4 particles near the surface layer is observed. The TEM images of the microstructure aged in air crystals at various magnifications, demonstrating the surface film, Ti_3Ni_4 particles near this film and the matrix away from the surface (Figure 6). The normal to the habit plane of oriented grown particles does not lie in the plane of the FIB film in Figure 6b,c.

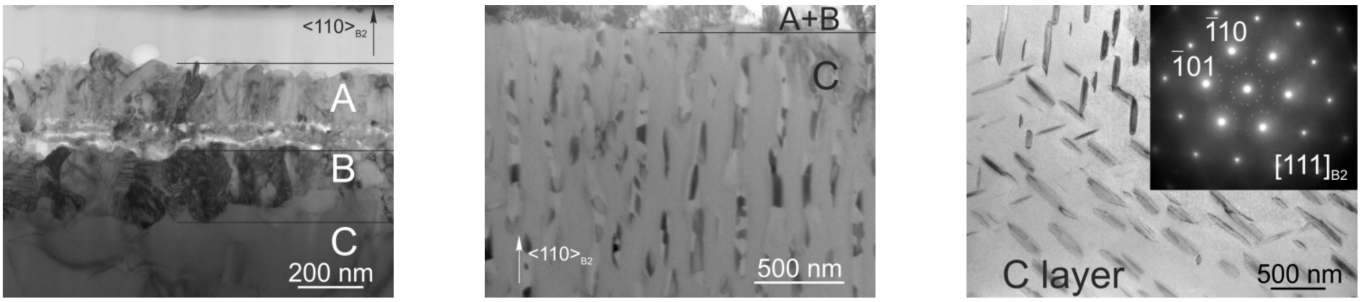

(**a**) (**b**) (**c**)

Figure 6. TEM study of $Ti_{49.3}Ni_{50.7}$ single crystals aged at 823 K for 1.0 h in air before fatigue tests: (**a**) bright field (BF) image of the surface film in the cross sections of sample; (**b**) BF image of B2-austenite and Ti_3Ni_4 particles near the surface film in the cross sections of sample and (**c**) BF image of B2-austenite and Ti_3Ni_4 particles and the correspondent selected area electron diffraction pattern (SAEDP) in the center of the sample.

The dispersed Ti_3Ni_4 particles have a lenticular shape and also create internal stresses in the matrix [26]. Oriented particle growth occurs so that the stresses in the matrix caused by particles compensate for the stresses (internal or externally applied stresses) in the material. This has been predicted theoretically and repeatedly confirmed experimentally [26–28]. Therefore, such an oriented particles growth near the surface film may be the way of relaxing the internal stresses created by the surface film in single crystals. Therefore, we

observe a weak effect of the oxide layer on the MT temperatures in the cooling/heating cycles in the stress-free state.

The studied $[001]_{B2}$-oriented crystals with and without an oxide layer demonstrate a good cyclic stability during loading/unloading cycles compared with the $[111]_{B2}$-oriented single crystals and polycrystals [5,29,30]. In $[111]_{B2}$-oriented single crystals the SE curves change, with an increase in the number of cycles by reducing the reversible strain, and become a straight line after 100 during loading/unloading cycles.

The SE response stability during cyclic tests in $[001]_{B2}$-crystals is explained by the high level of strength properties of the B2-phase $\sigma_{cr}(M_d) > 1000$ MPa [4,19]. However, local plastic deformation of the matrix is observed with the formation of both the dislocations near Ti_3Ni_4 particles and the residual martensite with fine twinned structure in the first 30 cycles (Figure 7b,c). This contributes to the martensite nucleation in subsequent cycles and reduces the critical stress σ_{cr} and hysteresis $\Delta\sigma$.

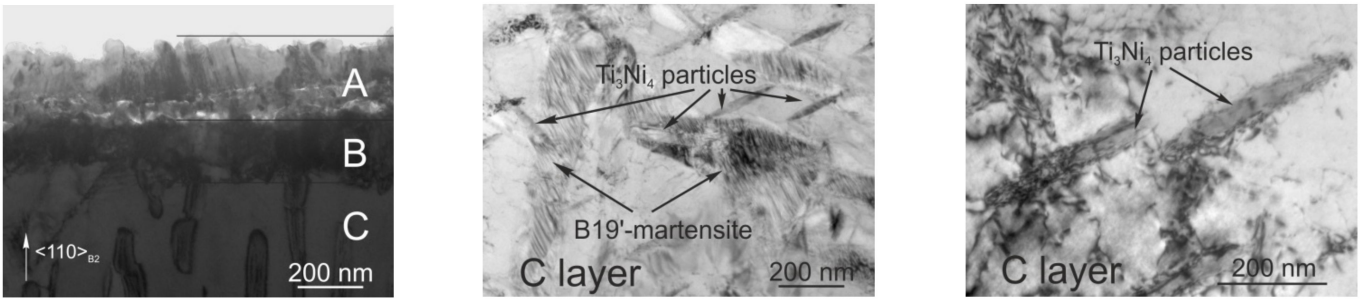

(**a**) (**b**) (**c**)

Figure 7. TEM study of $Ti_{49.3}Ni_{50.7}$ single crystals after fatigue tests: (**a**) BF image of the surface film in the cross-sections of sample (aged at 823 K for 1.0 h in air); BF images demonstrating (**b**) the residual B19′-martensite and (**c**) the dislocations near Ti_3Ni_4 particles (aged at 823 K for 1.0 h in helium).

The oxide layer is usually brittle, and does not undergo MT in contrast to the matrix. Whereas, after compressive fatigue tests of studied $[001]_{B2}$-crystals aged in air, no cracking of the oxide layer was found in (Figures 6a and 7a). Thus, the [001]-crystals aged in air, containing dispersed Ti_3Ni_4 particles and outer protective oxide layer, exhibit generally good cyclic stability.

The physical reason of a good SE behavior without cracking of the surface oxide layer during cyclic tests is related to several facts. First, the formation of a thin Ni-free layer ~250 nm, which reduces both the ratio of the surface layer volume to the material volume and the layer cracking probability in contrast to the thick layers (over 100 μm) [10,12,13]. Second, the formation of the surface layer simultaneously with the precipitation of dispersed Ti_3Ni_4 particles. The presence of dispersed Ti_3Ni_4 particles that do not undergo MT facilitates the relaxation of high internal stresses arising during the development of MT in the matrix, which is positive for film integrity. It is assumed that the relaxation of internal stresses created by both the oxide layer and matrix strain at the stress-induced MT occurs due to: (i) the oriented growth of Ti_3Ni_4 particles near a thin surface film at single crystals aged in air; (ii) the formation of a Ni-rich sublayer at single crystals aged in air; (iii) the formation of dislocations near the particle-matrix surface and a fine twinned structure of B19′-martensite, whose growth is limited by the distance between Ti_3Ni_4 particles during the stress-induced MT at cyclic tests. The precipitation of Ti_3Ni_4 particles with an interparticle distance of no more than 500 nm contributes to the "multiple" (turbulent) MT behavior. The "particle-matrix" boundaries are the predominant places for the martensite nucleation. Therefore, the nucleation and growth of B19′-martensite crystals occur simultaneously in different regions of the sample. This results in a homogeneous deformation of the sample and the absence of localized deformation at stress-induced MT [4]. That could explain the relatively large strain without cracking inside the oxide layer.

It should be noted that the surface film consists of two sublayers, contains pores and has a complex deformation mechanism at stress-induced MT. Additional studies are necessary to explain the mechanisms of deformation inside the oxide layer and Ni-rich sublayer during the stress-induced MT in the matrix.

5. Conclusions

The oxidation, oriented along the $[001]_{B2}$-direction $Ti_{49.3}Ni_{50.7}$ single crystals due to aging at 823 K for 1.0 h in air, makes it possible to obtain a Ni-free (78.0($\pm$1.9) at. % O, (21.8($\pm$0.6) at. % Ti) protective thin oxide layer (250 nm). The high-nickel layer with a thickness of ~170 nm is formed between the surface oxide layer and the matrix of material.

The formation of an oxide layer leads to the appearance of internal compressive stress in the matrix and the oriented growth of Ti_3Ni_4 particles near a thin surface film after aging in air.

The matrix of $Ti_{49.3}Ni_{50.7}$ single crystals aged in air and helium undergoes a two-stage B2-R-B19′ MT. The oxide layer has a weak effect on the B2-R-B19′ MT temperatures and does not worsen the SE response in $[001]_{B2}$-oriented $Ti_{49.3}Ni_{50.7}$ single crystals in compression. The weak influence of an oxide layer on the MT temperature and the absence of influence of an oxide layer on the SE properties is associated with the formation of a fine oxide layer together with the precipitation of Ti_3Ni_4 particles and the relaxation of internal stresses by the oriented arrangement of Ti_3Ni_4 particles near the surface film in $Ti_{49.3}Ni_{50.7}$ single crystals aged in air.

The oriented along the $[001]_{B2}$-direction $Ti_{49.3}Ni_{50.7}$ single crystals aged in helium and in air demonstrate high cyclic stability of the SE response, which does not depend on the presence of an oxide layer. Moreover, the oxide layer does not crack at cyclic tests due to the relaxation of internal stresses arising during the stress-induced MT at cyclic tests in aged single crystals. The main degradation of SE response is observed in the first 30 cycles and is associated with the formation of both the dislocations near Ti_3Ni_4 particles and the residual B19′-martensite with fine twinned structure.

The oxidation, oriented along the $[001]_{B2}$-direction $Ti_{49.3}Ni_{50.7}$ single crystals due to the aging at 823 K for 1.0 h in air, makes it possible to obtain a Ni-free protective thin oxide layer without negative change of the SE response and destruction of this layer during fatigue tests. This contributes to good biocompatibility of implants created on the basis of these materials.

Author Contributions: Conceptualization, E.Y.P.; Data curation, A.S.E. and E.Y.P.; Investigation, A.S.E., I.D.F. and M.N.V.; Methodology, I.D.F. and A.I.T.; Project administration, A.S.E.; Resources, M.N.V. and Y.I.C.; Supervision, E.Y.P. and Y.I.C.; Validation, A.S.E. and I.D.F.; Visualization, A.S.E. and I.D.F.; Writing—original draft, A.S.E.; Writing—review & editing, E.Y.P., A.I.T. and Y.I.C. All authors have read and agreed to the published version of the manuscript.

Funding: This research was funded by grant under the Decree of the Government of the Russian Federation No. 220 of 9 April 2010 (Agreement No. 075-15-2021-612 of 4 June 2021).

Data Availability Statement: The data used in this article are presented in the manuscript.

Acknowledgments: Electron microscopy studies were carried out on the equipment of the Krasnoyarsk Regional Center for Collective Use of the Kirensky Institute of Physics, Siberian Branch, Russian Academy of Sciences.

Conflicts of Interest: The authors declare no conflict of interest.

References

1. Jani, J.M.; Leary, M.; Subic, A.; Gibson, M.A. A review of shape memory alloy research, applications and opportunities. *Mater. Des.* **2014**, *56*, 1078–1113. [CrossRef]
2. Shao, M.; Cui, C.; Yang, H. Surface oxidation as the modification technique of NiTi shape memory alloys for medical application: A technological review. *Cailiao Daobao/Mater. Rev.* **2018**, *32*, 1181–1186. [CrossRef]
3. Nematzadeh, F. A computational study on the effect of bending number on superelastic behavior of NiTi for medical application. *J. Intell. Mater. Syst. Struct.* **2020**, *31*, 2117–2127. [CrossRef]

4. Timofeeva, E.E.; Panchenko, E.Y.; Zherdeva, M.V.; Eftifeeva, A.S.; Surikov, N.Y.; Tagiltsev, A.I.; Chumlyakov, Y.I. Effect of one family of Ti_3Ni_4 precipitates on shape memory effect, superelasticity and strength properties of the B2-phase in high-nickel [001]-oriented Ti-51.5 at.%Ni single crystals. *Mater. Sci. Eng. A* **2022**, *832*, 142420. [CrossRef]
5. Gall, K.; Maier, H.J. Cyclic deformation mechanisms in precipitated NiTi shape memory alloys. *Acta Mater.* **2002**, *50*, 4643–4657. [CrossRef]
6. Kaya, I.; Karaca, H.E.; Souri, M.; Chumlyakov, Y.; Kurkcu, H. Effects of orientation on the shape memory behavior of $Ni_{51}Ti_{49}$ single crystals. *Mater. Sci. Eng. A* **2017**, *686*, 73–81. [CrossRef]
7. Timofeeva, E.E.; Surikov, N.Y.; Tagiltsev, A.I.; Eftifeeva, A.S.; Neyman, A.A.; Panchenko, E.Y.; Chumlyakov, Y.I. The superelasticity and shape memory effect in Ni-rich Ti-51.5at.%Ni single crystals after one-step and two-step ageing. *Mater. Sci. Eng. A* **2020**, *796*, 140025. [CrossRef]
8. Hassel, A.W. Surface treatment of NiTi for medical applications. *Minim. Invasive Ther. Allied. Technol.* **2004**, *13*, 240–247. [CrossRef]
9. Chu, C.L.; Wu, S.K.; Yen, Y.C. Oxidation behavior of equiatomic TiNi alloy in high temperature air environment. *Mater. Sci. Eng. A* **1996**, *216*, 193–200. [CrossRef]
10. Firstov, G.S.; Vitchev, R.G.; Kumar, H.; Blanpain, B.; Humbeeck, J.V. Surface oxidation of NiTi shape memory alloy. *Biomaterials* **2002**, *23*, 4863–4871. [CrossRef]
11. Cissé, O.; Savadogo, O.; Wu, M.; Yahia, L.H. Effect of surface treatment of NiTi alloy on its corrosion behavior in Hanks' solution. *J. Biomed. Mater. Res.* **2002**, *61*, 339–345. [CrossRef] [PubMed]
12. Shabalovskaya, S.A.; Tian, H.; Anderegg, J.W.; Schryvers, D.U.; Carroll, W.U.; Humbeeck, J.V. The influence of surface oxides on the distribution and release of nickel from Nitinol wires. *Biomaterials* **2009**, *30*, 468–477. [CrossRef] [PubMed]
13. Mahmud, A.; Wu, Z.; Zhang, J.; Liu, Y.; Yang, H. Surface oxidation of NiTi and its effects on thermal and mechanical properties. *Intermetallics* **2018**, *103*, 52–62. [CrossRef]
14. Nam, T.H.; Chung, D.W.; Lee, H.W.; Kim, J.H.; Choi, M.S. Effect of the surface oxide layer on transformation behavior and shape memory characteristics of Ti-Ni and Ti-Ni-Mo alloys. *J. Mater. Sci.* **2003**, *38*, 1333–1338. [CrossRef]
15. Shabalovskay, S.; Anderegg, J.; Humbeeck, J. Van Critical overview of Nitinol surfaces and their modifications for medical applications. *Acta Biomater.* **2008**, *4*, 447–467. [CrossRef]
16. Neelakantan, L.; Swaminathan, S.; Spiegel, M.; Eggeler, G.; Hassel, A.W. Selective surface oxidation and nitridation of NiTi shape memory alloys by reduction annealing. *Corros. Sci.* **2009**, *51*, 635–641. [CrossRef]
17. Ng, C.W.; Mahmud, A.S.; Ahmad, M.N.; Razali, M.F.; Liu, Y. Estimation of titanium oxide layer thickness on thermally oxidized NiTi alloy based on color variations. *Mater. Werkst.* **2022**, *53*, 47–55. [CrossRef]
18. Undisz, A.; Schrempel, F.; Wesch, W.; Rettenmayr, M. Mechanism of oxide layer growth during annealing of NiTi. *J. Biomed. Mater. Res. A* **2012**, *100*, 1743–1750. [CrossRef]
19. Sehitoglu, H.; Karaman, I.; Anderson, R.; Zhang, X.; Gall, K.; Maier, H.J.; Chumlyakov, Y. Compressive response of NiTi single crystals. *Acta Mater.* **2000**, *48*, 3311–3326. [CrossRef]
20. Sehitoglu, H.; Jun, J.; Zhang, X.; Karaman, I.; Chumlyakov, Y.; Maier, H.J.; Gall, K. Shape memory and pseudoelastic behavior of 51.5%Ni–Ti single crystals in solutionized and overaged state. *Acta Mater.* **2001**, *49*, 3609–3620. [CrossRef]
21. Guo, W.; Steinbach, I.; Somsen, C.; Eggeler, G. On the effect of superimposed external stresses on the nucleationand growth of Ni_4Ti_3 particles: A parametric phase field study. *Acta Mater.* **2011**, *59*, 3287–3296. [CrossRef]
22. Zotov, N.; Pfund, M.; Polatidis, E.; Mark, A.F.; Mittemeijer, E.J. Change of transformation mechanism during pseudoelastic cycling of NiTi shape memory alloys. *Mater. Sci. Eng. A* **2017**, *682*, 178–191. [CrossRef]
23. Xie, X.; Kan, Q.; Kang, G.; Li, J.; Qiu, B.; Yu, C. Observation on the transformation domains of super-elastic NiTi shape memory alloy and their evolutions during cyclic loading. *Smart Mater. Struct.* **2016**, *25*, 045003. [CrossRef]
24. Kan, Q.; Yu, C.; Kang, G.; Li, J.; Yan, W. Experimental observations on rate-dependent cyclic deformation of super-elastic NiTi shape memory alloy. *Mech. Mater.* **2016**, *97*, 48–58. [CrossRef]
25. Otsuka, K.; Ren, X. Physical metallurgy of Ti–Ni-based shape memory alloys. *Prog. Mater. Sci.* **2005**, *50*, 511–678. [CrossRef]
26. Li, J.-F.; Zheng, Z.-Q.; Li, X.-W.; Li, S.-C. Effect of compressive stress aging on transformation strain and microstructure of Ni-rich TiNi alloy. *Mater. Sci. Eng. A* **2009**, *523*, 207–213. [CrossRef]
27. Michutta, J.; Carroll, M.C.; Yawny, A.; Somsen, C.; Neuking, K.; Eggeler, G. Martensitic phase transformation in Ni-rich NiTi single crystals with one family of Ni_4Ti_3 precipitates. *Mater. Sci. Eng. A* **2004**, *378*, 152–156. [CrossRef]
28. Chen, L.Q.; Li, D.Y. Selective variant growth of coherent $Ti_{11}Ni1_4$ precipitate in a TiNi alloy under applied stresses. *Acta Mater.* **1997**, *45*, 471–479. [CrossRef]
29. Gloanec, A.-L.; Cerracchio, P.; Reynier, B.; Van Herpen, A.; Riberty, P. Fatigue crack initiation and propagation of a TiNi shape memory alloy. *Scr. Mater.* **2010**, *62*, 786–789. [CrossRef]
30. Tyca, O.; Hellera, L.; Vronkaa, M.; Šittnera, P. Effect of temperature on fatigue of superelastic NiTi wires. *Int. J. Fatigue* **2020**, *134*, 105470. [CrossRef]